
# Original

Rakoch, A.; Monakhova, E.; Khabibullina, Z.; Serdechnova, M.; Blawert, C.; Zheludkevich, M.; Gladkova, A.:
**Plasma-electrolytic oxidation of AZ31 and AZ91 magnesium alloys: comparison of coatings formation mechanism.**
In: Journal of Magnesium and Alloys. Vol. 8 (2020) 3, 587 - 600.

First published online by Elsevier: 09.07.2020

https://dx.doi.org/10.1016/j.jma.2020.06.002

Available online at www.sciencedirect.com

ScienceDirect

Journal of Magnesium and Alloys 8 (2020) 587–600

www.elsevier.com/locate/jma

Full Length Article

# Plasma electrolytic oxidation of AZ31 and AZ91 magnesium alloys: Comparison of coatings formation mechanism

A.G. Rakoch[a], E.P. Monakhova[a], Z.V. Khabibullina[a], M. Serdechnova[b], C. Blawert[b], M.L. Zheludkevich[b,c], A.A. Gladkova[a,*]

[a] *Department of Metal Protection and Surface Treatment, National University of Science and Technology 'MISiS', Leninskiy prospekt 4, 119049 Moscow, Russia*

[b] *Helmholtz-Zentrum Geesthacht, Centre for Materials and Coastal Research GmbH, Max-Plank Str.1, 21502 Geesthacht, Germany*

[c] *Faculty of Engineering, Kiel University, Kaiserstrasse 2, 24143 Kiel, Germany*

Received 22 January 2020; received in revised form 29 May 2020; accepted 11 June 2020
Available online 9 July 2020

**Abstract**

The growth kinetics of PEO coatings on AZ31 and AZ91 magnesium alloys were studied and correlated with their structure, compositions (phase and elemental) and corrosion resistance. It was established that the coatings have a two- (outer and anodic) or three-layer structure (outer, inner and anodic) depending on the treatment time. Briefly, at short treatment time only an anodic layer and outer layer exists. Growth of the outer PEO layer takes place due to the micro discharges, which occur in vertical pores and voids with spherical cross-section. If the time is increasing, and electrolyte inside of the pores is heating-up, etching of the Mg substrate and oxide film becomes more dominant and horizontal pores in the interface between coating and metal are formed. In the pores new anodic layer will form and at this time the formation of the third inner layer starts. The growth of the inner layer happens via the anodic film as a result of micro discharge ignition in the horizontal pores, accompanied by formation of plasma in numerous micro-voids of this layer. The coatings formed on AZ91 alloy are denser, than those on AZ31, which is related to the difference in the rates of inner layer growth and dissolving of oxides which are located at the bottom of the horizontal pores. Because of the lower Al content, the AZ31 substrate itself and the also the oxide films are less stable and tend to dissolve at a higher rate compared to AZ91.

Thus, it was demonstrated that a good corrosion resistance of the coatings was only obtained on AZ91 and if the average thickness of the coating is around 50 μm, correlating with the formation of a sufficiently dense inner layer. Knowing this mechanism, a new two-step treatment was suggested, combining the standard PEO treatment with a subsequent PEO process in an electrolyte supporting the inner film formation. The concept was successfully applied and a further improved corrosion resistance was obtained compared to the single stage PEO process. This improvement of corrosion resistance was related to the better sealing of porosity and formation of a denser inner layer.


*Keywords:* Plasma electrolytic oxidation; Magnesium alloys; Coating formation; Coating growth; Corrosion resistance.

## 1. Introduction

Magnesium alloys are widely used in transport and 3C industries due to their low density, high-strength/weight ratio and damping capacity [1–7]. However, low corrosion resistance significantly limits their broad industrial use. Therefore, magnesium alloys must be appropriately protected prior to service in order to guarantee sufficient corrosion resistance.

The most popular methods of corrosion protection for magnesium alloys are based on the formation of stable oxide layers on their surfaces with further application of paints, enamels or any other top coatings [4,8]. As a result, plasma electrolytic oxidation (PEO) has received a great attention as one of the most effective ways for corrosion and wear protection of magnesium alloys [2,9–15]. This method is environ-

* Corresponding author.
*E-mail address:* sascha-gladkova@yandex.ru (A.A. Gladkova).

https://doi.org/10.1016/j.jma.2020.06.002

mentally friendly and the treatment is normally performed in aqueous solutions without additives of toxic compounds. The most widely used electrolytes to obtain hard wear-resistant PEO coatings are alkaline phosphate-aluminate based electrolytes [4].

The formation of PEO coatings is possible on almost all cast and wrought magnesium alloys [4,16,17]. However, PEO coating formation on magnesium alloys, including AZ31 and AZ91, in comparison with aluminum and titanium has some specific features. For example, it proceeds in different stages [1,18–20] and results in a formation of two- or three-layer coatings.

A number of different mechanisms of inner and outer layer formation were suggested in order to explain the appearance of plasma microdischarges as well as their type. For example, Tu et al. [21] suggested that the energy release in the microdischarge channels during PEO treatment of AZ31 is high enough to melt the coating materials beneath the outer layer. This results in the microstructure difference between inner and outer layers. Moreover, they indicate that big pores between these two layers are normally formed. From the author's point, these layers grow independently and the melted materials of the inner layer cannot penetrate into the outer layer of the PEO coatings [21]. This process takes place because of the high anodic current density (e.g. $10^4$ A/cm$^2$) within the transverse discharge channels causing a high energy release and melting of the coating materials beneath the outer layer. This results in extensive gas formation (most probably in ionized form [21]) and leads to appearance of pores in the coating between inner and outer layers [21].

Other studies [2,22–25] have also confirmed that the PEO coating formation on magnesium alloys is a multistage process. For example, in [22] it was shown, that the PEO coating formation on AZ31B took place in four stages. During the first stage, the anodizing process takes place, thus, an almost non-porous thin layer is formed (ca. 0.3 μm thickness). During the second stage the destruction of this layer and the formation of a porous one take place. During the third stage the coating thickness is not increasing, however, the already formed coating becomes denser (partial sealing of pores takes place). During the fourth stage the increase of coating thickness continues. The authors point out that two types of miscrodischarges and two different locations of their appearance exist. The first type of microdischarges appears at the bottom of voids between the metal substrate and the coating, while the second type occurs at the bottom of large pores. Later, leads to flaking off of the coating from the metal substrate. The initiation of all kinds of microdischarges takes place as a result of breakdown of dielectric oxide layers [22]. The authors do not consider the possibility of electrical breakdown of gas-vapor phase, which is forming in the pores of PEO coatings, as it was suggested by Günther-Schulze and Betz [26,27] as well as by other researchers [18–20,28,29]. Additionally, the presence of intermetallics ($Mg_{17}Al_{12}$) in the $\alpha$-Mg solid solution has a great influence on the PEO process behavior. For example, it was shown, that inhomogeneous growth of the PEO coating takes place [30–38] in the presence of $\beta$-phase ($Mg_{17}Al_{12}$).

Overall, porous PEO coatings, which are formed on magnesium alloys, provide normally poor corrosion resistance. Numerous attempts have been made in order to improve their protection capability e.g. by adding various particles (e.g. $ZrO_2$, $CeO_2$, $Al_2O_3$, SiC, $TiO_2$, $SiO_2$) into the electrolytes [39–48], changing processing parameters [49,50], *in-situ* sealing [51,52] and adjustment of phase composition of the coatings [53–57]. In spite of all these efforts, the corrosion resistance of the obtained coatings is still not sufficient, mainly because of vertical pores in the PEO coatings through which electrolyte can reach quickly the substrate.

It seems as if the studies about investigation of PEO process mechanisms of magnesium alloys do not take into consideration that neither the alloys nor the coatings are stable in hot concentrated aqueous alkaline solutions [22] and that horizontal pores are present in the coatings. The latter might be a result of dissolution of oxides circumjacent to the pores (example: MgO, $MgAl_2O_4$ and other double oxides). Overall, only a deep understanding of the PEO coatings formation mechanism will allow the development of protective coatings on different magnesium alloys. Thus, the aims of present study are:

(1) to identify the PEO coating growth mechanism on AZ31 and AZ91 magnesium alloys in alkaline phosphate-aluminate electrolyte as a function of treatment time;
(2) to find out the reasons for the difference in structure of the PEO coatings obtained on AZ31 and AZ91 magnesium alloys and in their corrosion resistances;
(3) to develop a method of synthesizing denser coatings with improved corrosion resistance on AZ31 and AZ91.

## 2. Experimental procedure

### 2.1. Materials

AZ31 and AZ91 magnesium alloys with a size of 0.5 and 0.35 dm$^2$, respectively, were used in frame of this work. Their chemical composition was determined using spark analysis (Spectrolab M9, Ametek-Spectro, Germany) and the results are given in Table 1.

AZ31 is mainly composed of $\alpha$ – Mg matrix and a few $Al_8Mn_5$ intermetallics, while AZ91 is composed of $\alpha$ – Mg matrix and a larger amount of $\beta$-phase ($Mg_{17}Al_{12}$).

The following chemicals were used for preparation of PEO electrolyte: sodium hydroxide (NaOH, p.a., OOO 'Component-Reaktiv', Russia), sodium phosphate ($Na_6P_6O_{18}$, SHMP 68%, 'Zhengzhou Qiangjin Science and Technol-

Table 1
Chemical composition of AZ31 and AZ91 magnesium alloys (wt%).

| Composition in wt% | Al | Zn | Mn | Be | Fe | Cu | Ni | Si |
|---|---|---|---|---|---|---|---|---|
| AZ31 | 3.04 | 1.00 | 0.27 | 0.00046 | 0.0028 | 0.0008 | 0.0010 | 0.020 |
| AZ91 | 8.16 | 0.72 | 0.40 | 0.001 | 0.03 | 0.06 | 0.007 | 0.10 |

ogy Trading Co., Ltd.', China), sodium aluminate ($NaAlO_2$, pur., ZAO 'Unikhim', Russia), technical water glass (TWG: $Na_2O \cdot 2{,}9\ SiO_2 \cdot 18H_2O$, pur., OOO 'Bit Servis Akva', Russia). Sodium chloride (NaCl, pur., OOO 'KhimSoyuz', Russia) was used for the solution for corrosion testing, while deionised water was used as a solvent for preparation of all solutions.

### 2.2. PEO process conditions

In frame of this work, most of the PEO experiments were conducted in aqueous solutions, containing 2 g/l NaOH, 3 g/l $Na_6P_6O_{18}$, and 5 g/l $NaAlO_2$. This electrolyte is defined as 'basic electrolyte'. Alkali-phosphate-aluminate electrolytes are widely used for PEO treatments to obtain corrosion resistant and hard coatings [1,4]. Prior to the PEO treatments, magnesium samples were rinsed in water and dried under air. During PEO in the basic electrolyte, an alternating current with a density of 10 A/dm$^2$ was applied. Such current densities are widely used to obtain protective coatings on magnesium alloys [4].

However, in order to improve corrosion resistance of PEO coatings, the following PEO electrolytes and conditions were also applied:

(1) aqueous solution, containing 180 g/l of technical water glass (TWG: $Na_2O \cdot 2.9\ SiO_2 \cdot 18H_2O$) and a current density equal to 1 A/dm$^2$. This electrolyte is widely used in order to form corrosion resistant amorphous coatings of silicon oxide on aluminum alloys [18];
(2) two-stage PEO treatment with the first stage conducted in the basic electrolyte with a current density of 10 A/dm$^2$ until the coating thickness reaches a value of ca. 20 μm and a subsequent second stage in aqueous solution, containing 180 g/l TWG, with a current density equal to 1 A/dm$^2$.

After the PEO treatment, samples were rinsed with deionized water and dried under air.

PEO treatment was conducted using a using 50 Hz (AC regime) bipolar capacitive PEO power supply manufactured by NUST MISiS, previously described in detail [58]. In order to keep the temperature of the working electrolyte in a range between 19 and 21 °C, a heat exchanger, consisted of AISI 304 (X18H10 RU) steel sheets and a microprocessor-controlled measuring equipment TPM−1'OVEN' (OOO SANA-TEK, Russia), was used. The electrolyte was circulated between the treatment bath and the heat exchanger device.

A digital camera Canon 550D with an exposure time of 10 msec was used for photographic recording of the anodic plasma microdischarges at the different stages of the PEO processes in the different electrolytes.

The pH of the electrolytes was measured using 'pH 211' pH-meter (HANNA Instruments, USA) The pH values were11.7 for basic electrolyte and 11.4 for the aqueous solution, containing 180 g/l TWG. The total volume of the electrolytes was constantly adjusted to 10 L and the temperature of the electrolyte was controlled in a narrow range of 19.5 ± 1.5 °C.

### 2.3. Material characterization

The thicknesses of the coatings were measured at 20 randomly selected locations using a thickness gauge 'Dualscope FNP10 Coating Thickness Gauge' (Fischer, Germany) and the average values were calculated. The device was calibrated using uncoated substrate material.

For the cross-section analysis and electrochemical measurements, the samples were mount in an 'Epomet Molding Compound' epoxy resin ('Buehler', Germany) using an automatic forcing press 'SimpliMet 1000' ('Buehler', Germany) and ground with successive grades of SiC abrasive papers until 2500 grid and finally polished with a diamond paste (1 μm) using grinding-and-polishing machine 'Vector PhoenixBeta' ('Buehler', Germany).

Cross-section morphology of PEO coatings were examined by scanning electron microscopy using a Tescan VEGA3 SB instrument (SEM, Brno, Czech Republic) and the elemental composition of the coatings were studied at different places using *X-act* energy dispersive X-ray (Oxford instruments, UK) spectrometer.

The phase composition was investigated using Bruker D8 Advance X-ray diffractometer (Karlsruhe, Germany). The measurements were carried out using Cu K$\alpha$ radiation in the range of 2 theta from 10° to 80° (exposure time 1 s, step 0.02°) under 3° incident angle. The specimens were rotated with a rate of 20 rpm.

Corrosion testing of the coatings was performed according to GOST 9.308–85 (Part 9 – alternating exposure in corrosive media) standard requirements. The specimens were alternatingly immersed in a 3 wt% NaCl solution for 10 min at room temperature and further 50 min in air with observations of the first release of hydrogen bubbles and the first visible pit appearance.

All electrochemical measurements were performed in a 3 wt% NaCl solution at a temperature of 25 ± 0.5 °C, using a three-electrode configuration, with a Ag/Ag–Cl reference electrode and a platinum-coated titanium counter electrode. The sample to be examined was operated as the working electrode. To perform the measurements, IPC-Pro 3A digital potentiostat (OOO NTF 'VOLTA', Russia) was used and controlled by IPC-2000 software. Anodic polarization was performed in potentiodynamic mode with a potential scan rate of 1 mV/s. After obtaining the polarization curves, the values of the corrosion current were calculated by the Stern – Geary method [59].

Roughness of the coating surface (Ra) was evaluated via a portable surface roughness tester SURFTEST SJ-402 (Mitutoyo, Japan).

Air breakdown voltage in the coating pores was measured by a universal breakdown tester UPU-6 (OOO 'PKF Molniya', Ukraine) using rectified voltage with negative polarity. According to GOST 6433.3-71 the temperature was 20 °C

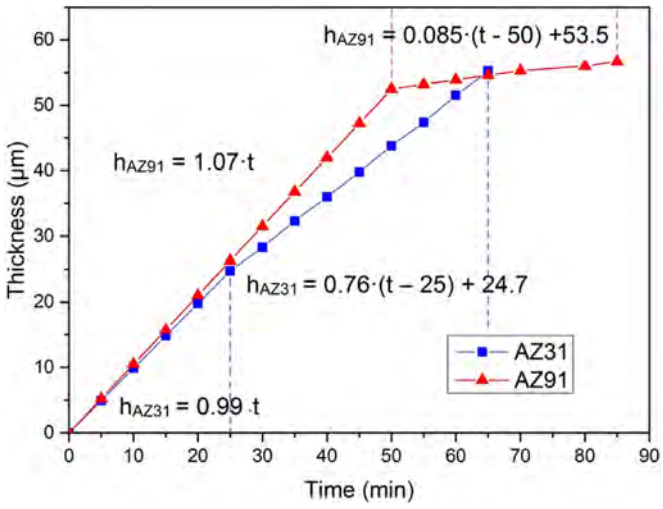


Fig. 1. Kinetics of PEO coatings growth on AZ31 and AZ91 alloys in alkaline phosphate-aluminate electrolyte.

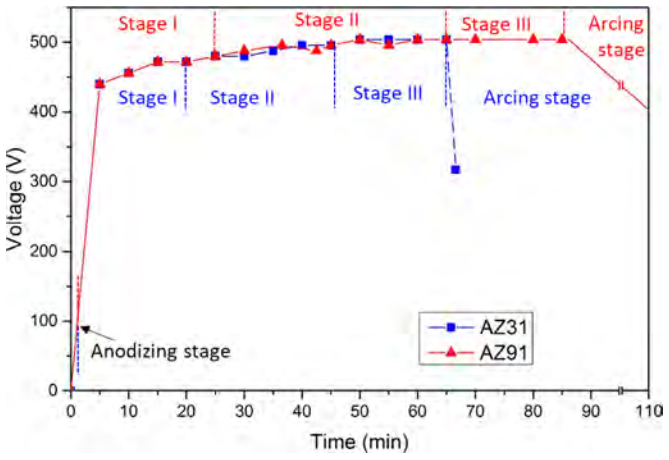


Fig. 2. The evolution of voltage as function of time during PEO treatment of AZ91 and AZ31 magnesium alloys in alkaline phosphate-aluminate electrolyte.

and the humidity 55% determined by a digital thermometer-hygrometer Mini Digital KAMEEL (Nanchang Huatuo Industrial Co., Ltd., China). Prior to measurements samples were ground with successive grades of SiC abrasive papers (P-Grade from P360 to P4000) up to 1.5–1.7 μm and rinsed with tap water followed by deionized water and dried under air. The coatings thickness losses did not exceed 6 μm.

All results given in this study are taken from a set of experimental data of at least five measurements.

## 3. Results and discussion

### *3.1. PEO treatment of AZ91 and AZ31 alloys in alkaline phosphate-aluminate electrolyte*

#### *3.1.1. Growth kinetics*

The thickness of the PEO coatings as function of treatment time on AZ31 and AZ91 magnesium alloys is shown in Fig. 1. It can be seen, that the average growth rate of PEO coating on AZ91 alloys in an alkaline phosphate-aluminate electrolyte is 1.07 μm/min in the first 50 min of the treatment and changes to 0.08 μm/min in the subsequent time period until 85 min. For AZ31 the initial growth rate is 0.99 μm/min in the first 25 min of PEO treatment and slows down to 0.76 μm/min in the remaining period until 65 min.

However, in spite of different rates of coating formation, it can be seen, that the ‘voltage/time’ dependence during PEO processing of AZ91 and AZ31 alloys is similar (Fig. 2). A clear difference can be observed only at the moment, when the final arcing stage is reached and the thickness of the PEO coatings is around 55.0 and 56.5 μm for AZ31 and AZ91 alloys respectively.

#### *3.1.2. Structure, composition and morphology of the coatings*

Interestingly, in spite of almost the same ‘voltage-time’ dependence (Fig. 2) and relatively small difference in the average kinetics of the coating growth (Fig. 1), it can be seen that the microstructure of the obtained PEO coatings varies significantly especially for longer-duration PEO treatment of AZ91 and AZ31 alloys (Fig. 3).

Based on the cross section micrographs (Fig. 3), one can conclude that initially the coatings formed in alkaline-phosphate-aluminate electrolyte consist of two layers: an anodic film and an outer layer. If the time is increasing, three-layer coating is formed in the final stage: an anodic film, an inner and an outer layer. Based on XRD results, these layers mainly consist of MgO and $MgAl_2O_4$ (Fig. 4).

However, the amount of magnesium aluminate (spinel phase) in the inner layers of the coating formed on AZ91 seems to be higher than that for AZ31. This can be estimated from the comparison of the aluminium concentration closer to the interface for the two alloys (Fig. 5 and Table 2).

The surface morphology of the coatings synthesized on AZ31 and AZ91 alloys differs significantly. The coating sur-

Table 2
Elemental composition of the PEO coatings obtained on AZ31 and AZ91 (locations of analysis according to Fig. 5).

| Element | Elemental composition, wt% | | | | | | | | | | | | | |
|---|---|---|---|---|---|---|---|---|---|---|---|---|---|---|
| | Point 1 | Point 2 | Point 3 | Point 4 | Point 5 | Point 6 | Point 7 | Point 8 | Point 9 | Point 10 | Point 11 | Point 12 | Point 13 | Point 14 |
| Mg | 44.5 | 39.9 | 41.9 | 43.3 | 54.5 | 55 | 55.8 | 44.8 | 44.9 | 39.7 | 36.3 | 43.8 | 44.7 | 45.5 |
| O | 37.9 | 40.1 | 41.2 | 41.5 | 36 | 39.7 | 39.3 | 38.8 | 40.9 | 42.8 | 41.7 | 43.6 | 41.9 | 40.6 |
| Al | 13.8 | 17.8 | 13.7 | 12.8 | 5.3 | 4.1 | 3.9 | 15.4 | 12.4 | 11.8 | 11.2 | 9.4 | 7.7 | 10.3 |
| P | 3.8 | 2.2 | 3.2 | 2.4 | 4.2 | 1.2 | 1 | 1 | 1.8 | 5.7 | 10.8 | 3.2 | 5.7 | 3.6 |

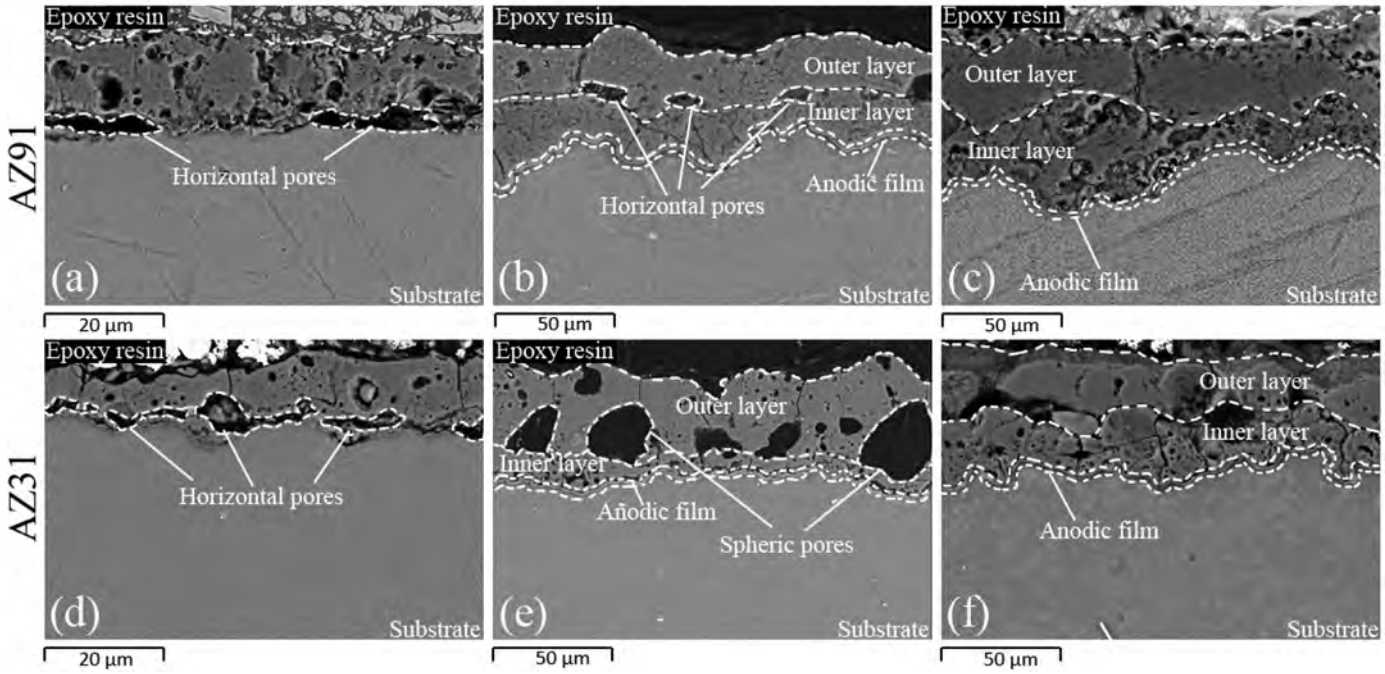


Fig. 3. SEM micrographs of cross section morphology of coatings with various thicknesses grown on the AZ91 (a)–(c) and AZ31 (d)–(f) alloys: *(a)* $21 \pm 2$ *μm or* 20 min *of treatment; (b)* $42 \pm 5.5$ *μm or* 40 min *of treatment; (c)* $54 \pm 6$ *μm or* 65 min *of treatment; (d)* $17 \pm 4$ *μm or* 20 min *of treatment; (e)* $40 \pm 3.5$ *μm or* 45 min *of treatment; (f) –* $53 \pm 4.5$ *μm or* 65 min *of treatment.*

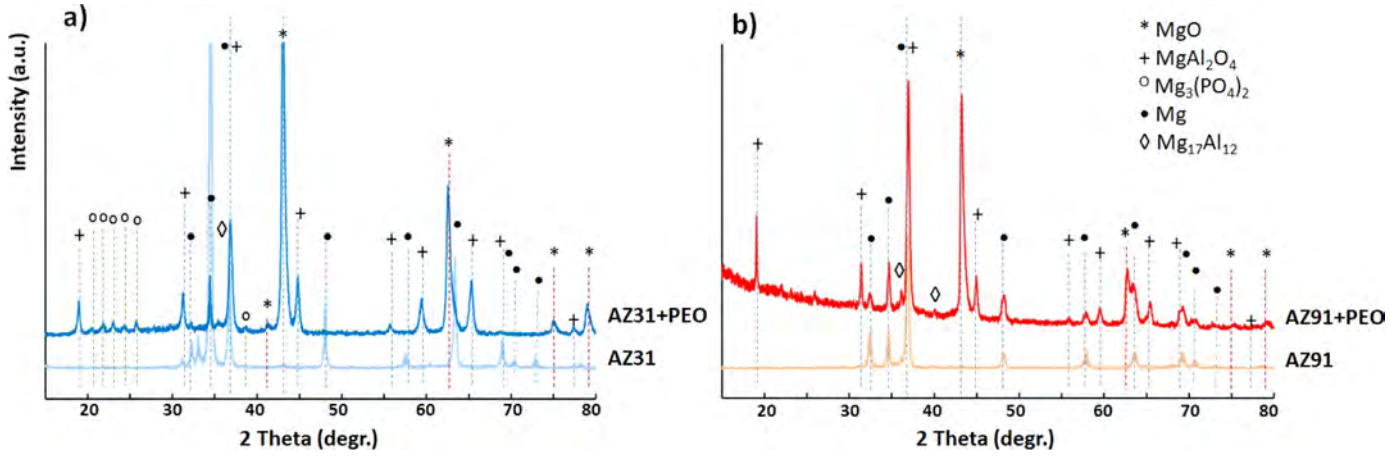


Fig. 4. XRD patterns of PEO coatings obtained on AZ31 (a) and AZ91 (b); average coating thickness is ca. 54 μm (65 min treatment time).

face topography on AZ91 is more uneven than that on AZ31 (Fig. 6).

### *3.1.3. Evolution of microdischarges and different stages during the PEO processing*

With increasing treatment time, changes in the appearance of the micro-discharges occur, which are visible by the naked eye (Fig. 7). Firstly, after a short time (< 1 min) a large number of easily distinguishable micro-discharges are ignited (Fig. 7(a)). Secondly, bright powerful micro-discharges are ignited after $9 \pm 2$ min (Fig. 7(b)). Afterwards, single, brightly burning micro-discharges are simultaneously present together with a large number of dull small micro-discharges, which appear after $30 \pm 2$ and $25 \pm 2$ min of PEO processing of AZ91 and AZ31 alloys, respectively (Fig. 7(c)). Finally, only dull small micro-discharges appear in larger number on the working electrodes after $50 \pm 3$ and $44 \pm 3$ min of PEO processing of AZ91 and AZ31 alloys, respectively (Fig. 7(d)).

The set of experimental data (Figs. 1–7) indicates a multistage formation of the coatings and a significant difference in formation and structure of the coatings synthesized on AZ31 and AZ91 magnesium alloys.

One can see that prior to formation of discharges, the anodizing of the metal substrate results in a significant increase in the anodic voltage (Fig. 2) [18–22].

Moreover, if the processing is stopped before the ignition of plasma discharges (anodic voltage reaches $180 \pm 5$ V), porous films are formed on the surface of AZ91 and AZ31

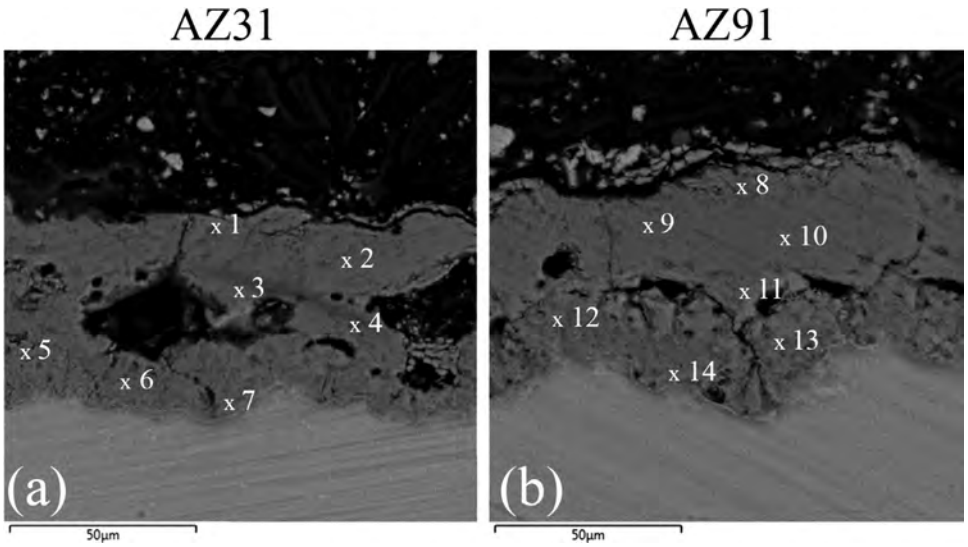


Fig. 5. SEM micrographs of cross section morphology of coatings grown on AZ31 (a) and AZ91 (b) in alkaline phosphate-aluminate electrolyte; average coating thickness is ca. 54 μm (65 min treatment time).

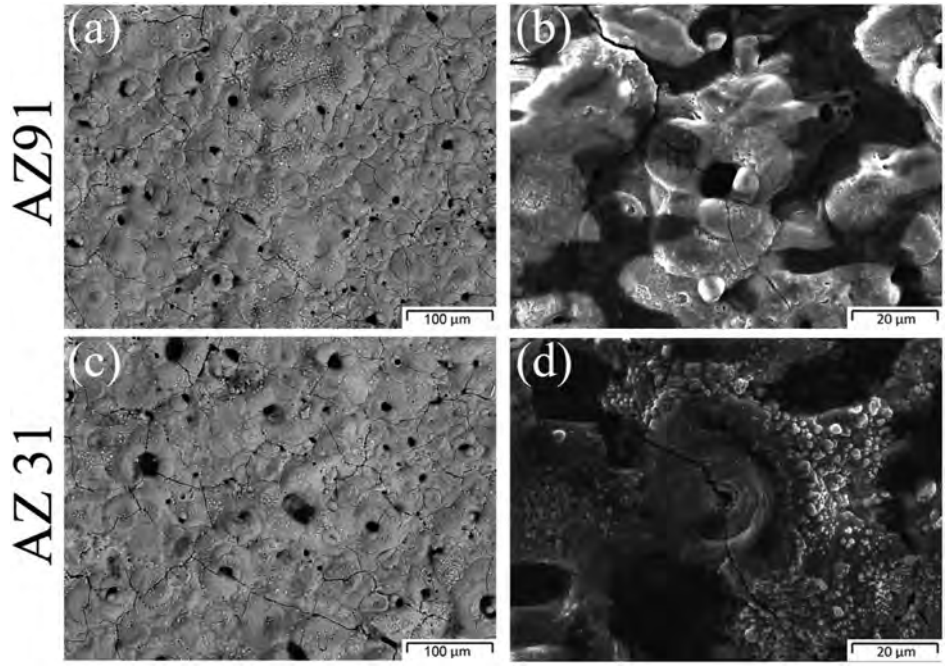


Fig. 6. The morphology of the PEO coatings on AZ91 (a) and (b) and AZ31(c) and (d). The average thickness of the coatings is ca. 54 μm (65 min treatment time).

alloys with an average coating thickness of $0.22 \pm 0.04$ and $0.27 \pm 0.03$ μm, respectively. Changes in the free corrosion potential of the magnesium alloys do not occur due to the presence of pores in the anodic film (Fig. 8 and Table 3). Moreover, no changes were observed in the time before first hydrogen bubble release (~ 0.02 min) and the first visible pit appearance (on the edges and corners after $5 \pm 2$, $14 \pm 3$ min and on the faces after $15 \pm 3$, $35 \pm 5$ min on AZ91 and AZ31, respectively) during immersion in a 3 wt% NaCl aqueous solution.. However, the density of pits on the anodic film surface decreases significantly. The last is consistent with the decrease of corrosion current density after anodizing of the magnesium alloys (Fig. 8).

Table 3
Corrosion currents and potentials of AZ31 and AZ91 alloys in a 3 wt% NaCl in Fig. 8.

| Alloy | Coating thickness, μm | I, A | -V, mV |
|---|---|---|---|
| AZ31 | 0 | $1.0 \cdot 10^{-4}$ | 1525 |
| AZ31 | $0.26 \pm 0.04$ | $1.5 \cdot 10^{-5}$ | 1535 |
| AZ91 | 0 | $3.0 \cdot 10^{-5}$ | 1480 |
| AZ91 | $0.3 \pm 0.03$ | $9.5 \cdot 10^{-6}$ | 1480 |

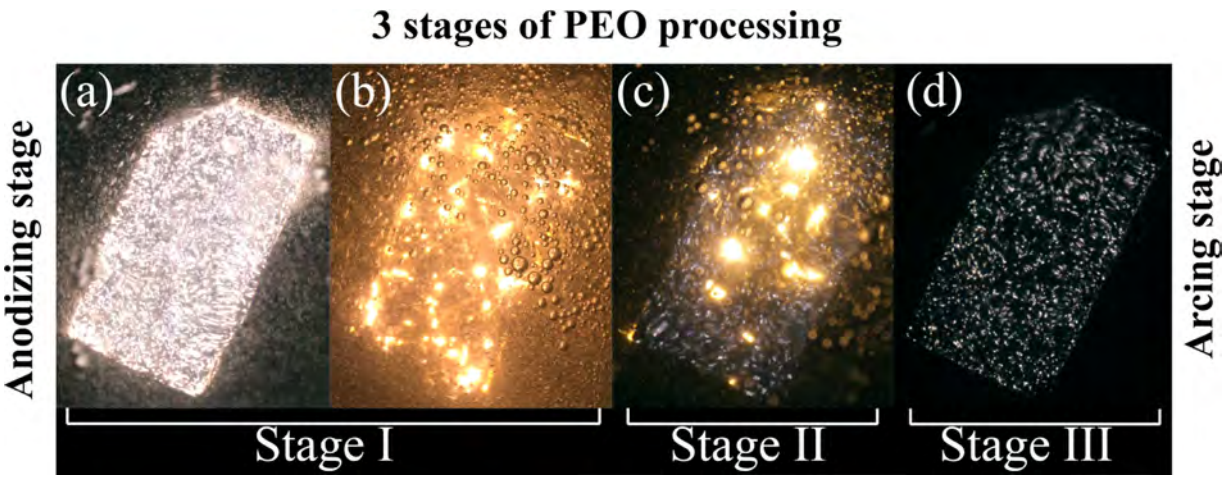


Fig. 7. A typical change in the appearance of microdischarges during PEO processing of AZ31 and AZ91 alloys in an alkaline phosphate-aluminate electrolyte with an increase in treatment time.

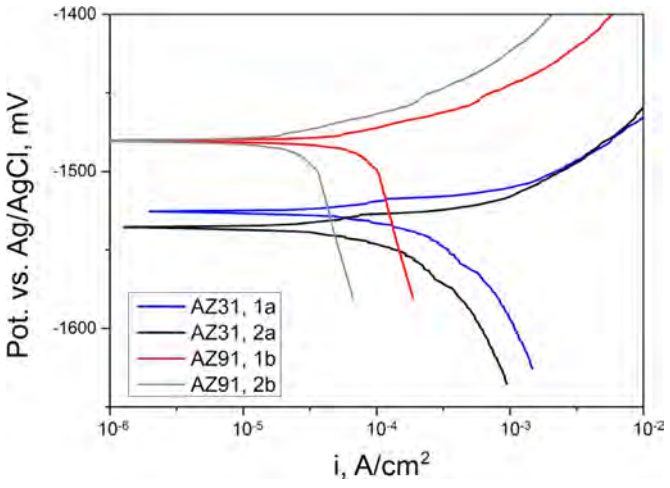


Fig. 8. Potentiodynamic polarization curves for the corrosion of AZ31 (1a, 2a) and AZ91(1b, 2b) alloys in a 3 wt% NaCl solution without (1a, 1b) and with the anodic coatings (2a, 2b): average coating thicknesses are ca 0.26 (2a), 0.3 (2b) μm.

During the first stage of PEO treatment, the growth of the coatings mainly occurs due to ignition of anodic plasma micro-discharges in vertical pores (Fig. 9(a)) leading to heating of the adjacent areas in the coating. Similar to PEO treatment of other alloys (aluminum [18], titanium [19], zinc [60]), the process involves several steps, including oxidation of the base metal, electrolysis of anions on the surface of the working electrode, and plasma-thermochemical treatment of the coatings. At this stage, due to the increase in power released in the micro-discharges, their brightness and size increase, while their density on the surface decreases (Fig. 7(b)). Visually it appears as if the microdischarges are moving across the surface of the working electrode.

The PEO layer formed in stage I is porous and electrolyte can reach the magnesium substrate throughout the existing vertical discharge channels. During a PEO treatment (using an AC power supply) in each period prior ignition of microdischarges or in areas where they are not occurring, the following two processes can take place:

(1) anodizing with further formation of a porous MgO film on the surface of the bare metal substrate;
(2) its simultaneous dissolution at temperatures above 60 °C [30–33,62] following Eq. (1) [63]:

$$MgO + 2OH^- + H_2O \rightarrow Mg(OH)_4^{2-} \quad (1)$$

The mechanism of formation of the anodic film in the horizontal pores of the coating is similar to that of sulfuric acid anodizing of aluminum alloy when the formation of the anodic film and its etching occur simultaneously [61].

The dissolution of MgO and $MgAl_2O_4$ circumjacent to horizontal pores leads to further widening of the pores (discharge channels).

Thus, the thin coatings (approximately up to 20 μm) obtained by PEO treatment in various electrolytes are all highly porous and include horizontal pores above the anodic film [2,4,16,17,21,22,61].

During the next stage (Stage II) of PEO processing, the probability of two competing processes increases. Please note, that the mechanisms differ for AZ31 and AZ91 from stage II, Fig. 9b,c shows a very early (Stage II-a) and a later moment (Stage II-b) during PEO processing of AZ91. Fig. 9(e) and (f) shows the same for AZ31. Simultaneously with formation of the outer layer, PEO also starts under this layer due to ignition of microdischarges in numerous pores (continuation of the anodic film pores) of the growing inner layer, accompanied by transportation of plasma to the horizontal pores (Fig. 9(c) and (f)). Thus, the microdischarges, igniting under the outer layer of the coating, lead to oxidation of the metal substrate, but do not transport the oxides towards the surface of the outer coating layer. They are forming an inner layer growing on the anodic film. During this stage, two types of microdischarges (dull small micro-discharges and brightly burning ones) are igniting on the surface of the working electrode (Fig. 7(c)).

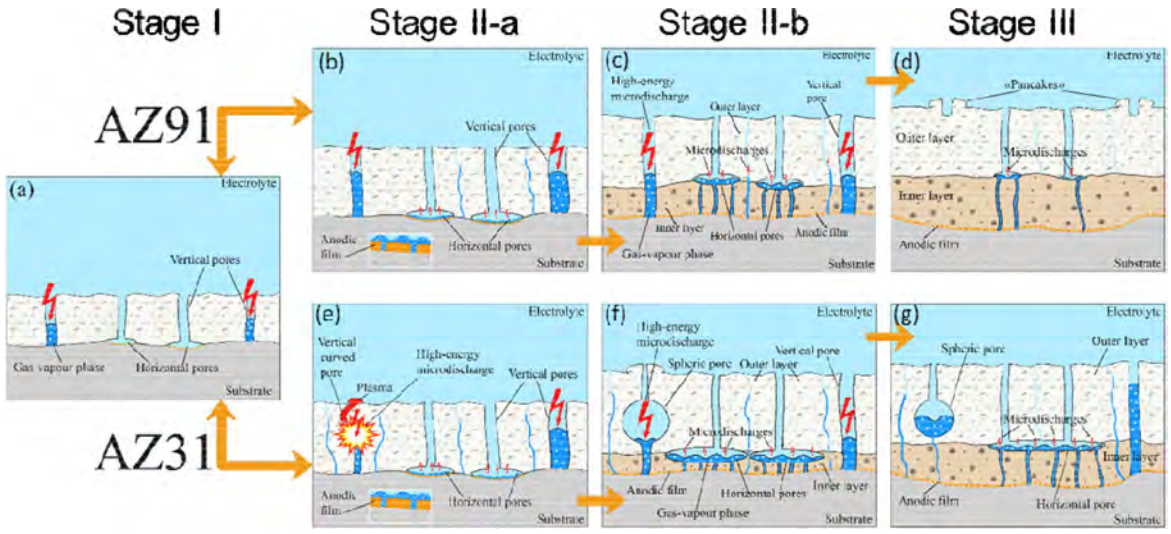


Fig. 9. Mechanisms and differences of coating formation via ignition of various types of micro discharges during PEO process of AZ31 and AZ91 magnesium alloys in alkaline phosphate–aluminate electrolyte.

During stage II-b, there is a high probability that sealing of the pores located above the coating inner layer or their "shifting" from the metal substrate toward the interface inner/outer layers will occur. This depends on the ratio between the coating inner layer growth rate ($\gamma_{\text{in.layer.}}$) and the circumjacent oxides dissolution rate ($\gamma_{\text{ox.diss.}}$). Higher dissolution rate of the existing oxides (located in the upper part of the horizontal pores) compared to the new oxide formation rates in the inner layer ($\gamma_{\text{in.layer.}}$) may result in only partial sealing of the pores, while inner plasma microdischarges are igniting.

In spite of a high similarity of the processes occurring during PEO treatment of AZ31 and AZ91 alloys, the ratio between $\gamma_{\text{in.layer}}$ and $\gamma_{\text{ox.diss.}}$ as well as the energies, released in the vertical pores during the process, differ a lot. This results in the observed different structures of the coatings.

During the second stage (Stage II-a) of PEO treatment of AZ31, formation of horizontal microvoids occurs at the metal substrate/coating interface, in curved vertical and bend pores (discharge channels) due to strong microdischarges. The diameter of the microvoids is much larger than the one of the pores (discharge channels). Release of large amount of formed gas (including gas in ionized form [21]) leads to formation of the microvoids in the outer layer (Figs. 3(e) and 9(f)). In most of the cases, the generated microvoids (Figs. 3(e) and 5(a)) have a circular cross section and hereafter these microvoids will be called as spherical pores.

Further PEO processing of AZ31 increases probability of microdischarges ignition at the bottom of the spherical pores, located in the coating outer layer (Fig. 7(c)). This process in stage II-b is accompanied by a release of high energy. The mechanism of high-energy microdischarge ignition can be explained by accumulation of the gases at the bottom of the spheric pores which form a dielectric gas layer. These gases release through the anodic film micropores and then through the micropores of the coating inner and outer layers during anodic and cathodic polarization of the working electrode and, thus, accumulate.

Table 4
Air breakdown voltages in the coating pores formed on AZ31 and AZ91 alloys ($U_{bd}$).

| Alloy | Coating thickness ($h$), μm | Breakdown voltage ($U_{bd}$), V | $U_{bd.}$/h*, V/μm | *Note |
|---|---|---|---|---|
| AZ31 | 17.7 ± 0.9 | 305 ± 15 | 17.2 | Conditional value of average electric strength for rectilinear pores |
| AZ31 | 29.9 ± 0.7 | 460 ± 20 | 15.4 | |
| AZ91 | 20.2 ± 0.5 | 270 ± 15 | 13.4 | |
| AZ91 | 30.4 ± 0.75 | 360 ± 20 | 11.9 | |

At the second stage, the inner layer has low growth rate due to the high energy release during ignition of the microdischarges in the spheric pores. As a results, $\gamma_{\text{ox.diss}}$. is higher than $\gamma_{\text{in.layer.}}$ and formation of the large voids in the coating at the inner\outer layers interface takes place (Figs. 3(e) and 9(f)).

Tu et al. [21] also report the ignition of microdischarges in the pores separating the inner and the outer layers. The authors believe that breakdown of dielectric oxide layers occur, however they do not provide any explanation of their formation in the microvoids.

PEO processing of AZ91, which has a large amount of big size $Mg_{17}Al_{12}$ intermetallics [30–33,62], leads to formation of vertical pores, which are less curved than those forming in AZ31, although the PEO treatment was conducted under the same conditions. The difference in the pore structure formed on AZ31 and AZ91 alloys can be demonstrated by measuring the air breakdown voltage of the coatings. The breakdown voltage for AZ31 is larger compared to AZ91 (Table 4). The higher values of the voltage are, the longer (more curved) pores were formed [64].

Formation of less curved pores is caused by the presence of intermetallics on the AZ91 alloy surface and ignition of

microdischarges above them [65]. As a result at stage II no spheric voids were formed in the coating outer layer (Figs. 3 and 5). Absence of spheric microvoids in the coating outer layer and more uneven surface topography of the coatings synthesized on AZ91 compared to AZ31 can be noticed as well (Fig. 6(b)). Unevenness of the coating surface topography on AZ91 is associated with transportation of the melted oxides onto the coating surface after the microdischarge ignition in its vertical pores. Thus, a pancake-like surface morphology is formed [21,66]. Moreover, roughness of the coatings formed on AZ91 ($R_A = 13\,\mu m$) is bigger than for AZ31 ($R_A = 9\,\mu m$). The latter is caused by ignition of powerful microdischarges in the spheric pores and loss of the melted oxides to the electrolyte (Fig. 6(d)). The meaningful role of the nature and concentration of secondary phases for the growth and structure of the coatings synthesized on magnesium alloys during PEO processing are also mentioned in literature [30–38].

Less use of energy for ignition of powerful microdischarges in spheric pores (compared to AZ31) results in a higher growth rate of the inner layer on AZ91 alloy. The latter is likely to be the main reason for the formation of thicker inner layers during PEO processing of AZ91 alloy (Fig. 3).

In stage III, when the coating thickness exceeds $37.5 \pm 5.0$ for AZ31and $54.5 \pm 5.5\,\mu m$ for AZ91, only microdischarges with weak intensity can be observed (high-energy microdischarges disappear) on the surfaces (Fig. 7(d)). This can be explained by an increase of temperature in the 'alloy-coating-electrolyte' system, which results in an increase of the volume of gas-vapor phase in the vertical pores (discharge channels) and spherical voids. At this moment, the microdischarges are taking place only under the coating outer layer (Fig. 9(d) and (g)). At this stage, mainly sealing of the pores in the coating inner layer on AZ91 occurs, while on AZ31 growth of the inner layer dominates. The latter can also be seen in the cross-section morphology of the coatings (Fig. 3(c) and (f)). Furthermore, at this stage the average growth rates of the coatings on AZ91 ($\sim 0.08\,\mu m$/min) is much lower than for AZ31 ($\sim 0.76\,\mu m$/min).

However, with further continuation of PEO treatment of AZ31, the process reaches a state of uncontrolled arcing (stage IV), when the average coating thickness exceeds $55.5\,\mu m$. The results is the formation of macro size defects in the coating. The transition is accompanied by a short-term noise effect, followed by a drop of voltage (Fig. 2) and an increase in current density (from 10 to about 14 A/dm$^2$). Most probably, this can be explained by the anodic voltage exceeding the breakdown potential of the gas-vapor phase in one or more vertical pores or spheric voids. Such microdischarges in single vertical or spherical pore(s) are accompanied by a high energy release, destroying the coating.

The same happens also for AZ91 when the average coating thickness exceeds $56.5\,\mu m$. However the anodic voltage drops less drastically as in the case of AZ31 alloy (Fig. 2). At the arcing stage of PEO processing of AZ91, the change in electrical characteristics is not accompanied by an increase of noise. A possible explanation can be an increase of temperature in the coating inner layer, which increases locally the dissolution rate of this layer and in the anodic film, whereby areas of the bare substrate appear. Thus, less voltage is needed to drive the process.

Summarizing, the inner layer is the most important and dense part of the coating, which determines obviously its properties. To obtain coatings with good corrosion properties, the process can be either stopped at the right moment or a two-step PEO treatment can be performed to seal the defects. The second step treatment should utilize an electrolyte, which strongly supports discharges in the inner layer.

### 3.2. Two-step PEO treatment of AZ31 and AZ91 alloys

It is well known [18] that the coatings obtained on aluminum alloys during PEO treatment at low current densities (up to 4 A/dm$^2$) in alkaline aqueous solutions with a high concentration of technical water glass (180 g/l) results in an excellent corrosion resistance. However, PEO treatment of magnesium alloys with a current density of 1 A/dm$^2$ switches to the arc stage already after 19 min of processing time with the formation of fragile phases on the surface of the coatings. In this case, the thickness of the coating differs significantly at different locations of the surface (from ca. 4.5 to $14\,\mu m$ on AZ91 alloy and from ca. 5.5 to $12.3\,\mu m$ on AZ31 alloy). The results indicate that there is a fast sealing of vertical pores in the coatings during PEO treatment of the alloys [67]. Strong energy release in the residual pores results in the transition to the arc stage and formation of macro size defects in the coatings [18,19].

However, if initially a PEO coating on magnesium alloys is produced in alkaline phosphate-aluminate electrolyte (in particular with a thickness of ca. $20\,\mu m$), and then subsequently the process is continued in an aqueous solution containing 180 g/l of TWG, many horizontal pores are sealed. As a consequence, microdischarges will take place mainly under the initial coating and instead of a transition to the arc stage, a formation and growth of an inner layer take place.

After the initial PEO coating with $19.5 \pm 3.5\,\mu m$ thickness was grown on the surface of AZ91, only dull small microdischarges ignite during the subsequent secondary PEO treatment at 1.0 A/dm$^2$ current density (Fig. 10). The average coating growth rate at a constant current density of 1 A/dm$^2$ is higher ($0.76\,\mu m$/min) on AZ91, while it does not exceed $0.50\,\mu m$/min during PEO treatment of AZ31. As shown in Fig. 10(a), there is still a mixture of discharges on AZ31, suggesting that not only the inner layer is growing.

The peak anodic voltages during the secondary PEO treatment of AZ91 and AZ31 alloys in the silicate electrolyte are lower than the ones in alkali-phosphate-aluminate electrolyte (Figs. 2 and 11). In the initial stage of the secondary PEO treatment, the voltage increases due to increase of coating temperature, which results in an increase of the volume of gas-vapor phase in the various pores. With further continuation of PEO treatment the temperature changes only slightly.

However, there is a significant decrease in the anodic voltage (Fig. 11) during the secondary PEO of AZ91 and AZ31

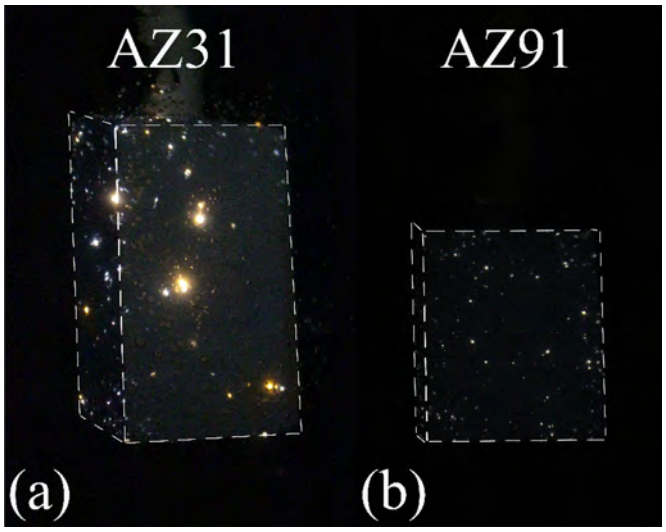


Fig. 10. A typical change in the type of microdischarges during the secondary PEO treatment of AZ31 (a) and AZ91 (b) alloys in alkaline-silicate electrolyte.

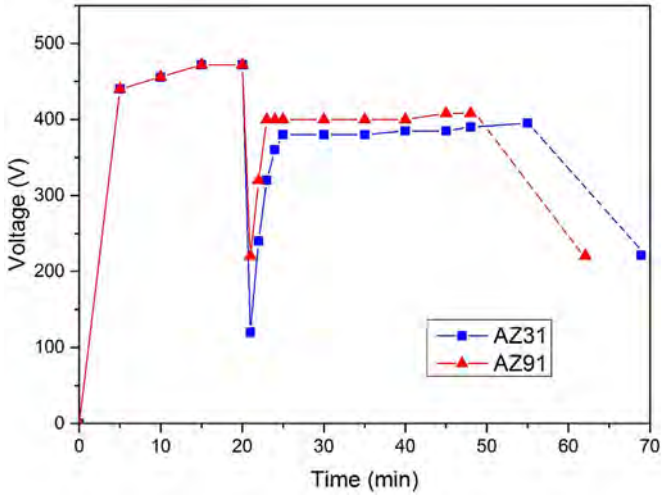


Fig. 11. The evolution of voltage as function of time during two-step PEO treatment of AZ31 and AZ91.

alloys after about 28 and 35 min, respectively. Presumably, etching of the inner layer and of the anodic film of the PEO coating takes place in localized regions. These processes are caused most likely by an increase of temperature and pH under the outer layer of the PEO coating.

Despite the high concentration of TWG in the aqueous solution, the concentration of silica-containing compounds in the coatings is relatively low (Fig. 12 and Table 5). The high amount of microdischarges accumulated locally in the inner layer of the coating leads to blocking of most of the coating surface by gas-vapor phase, which does not allow an intense electrolysis of $n[SixOy]^{m-}$ polyanions to this layer (Fig. 12 and Table 5). However, very small concentration of silicon containing compounds, most probably silicon oxide, could be found in the outer layer of the coating synthesized on AZ31 (Table 5). During PEO processing of this alloy, thermochemical transformation of $n[SixOy]^{m-}$ polyanions takes place above the outer layer stimulated by microdischarges igniting in the vertical and spheric pores of the outer layer. A lower amount of energy is used for growth of the coating inner layer due to consumption of high electric energy during ignition of the microdischarges in these voids. This explains why the thickness of the inner layer of the coating synthesized on AZ31 is thinner than on AZ91 (Fig. 12).

### *3.3. Anticorrosion properties of single- and double-step PEO treatments*

Although the conditions of PEO processing on AZ31 and AZ91 alloys were identical, the differences in the coating microstructures led to a different corrosion resistance. The coatings synthesized on AZ31 have lower corrosion resistance compared to AZ91 (Table 6). The corrosion resistance increases with duration of PEO treatment till the arcing stage of the process is reached. However, only coatings with average thicknesses from 53.5 to 56.5 μm grown on AZ91 alloy demonstrate a high corrosion resistance, which exceeds the requirements of GOST 9.308–85 (Part 9) [68] (Table 6). The formation of a relatively dense inner layer results in a significant increase of corrosion resistance (Fig. 3 and Table 6). The latter is also confirmed by the results obtained after the two-step PEO treatment (Table 7).

Moreover, the differences in the corrosion resistance of the magnesium alloys and the different coatings were proved by additional electrochemical measurements. Values of the corrosion current of AZ91 alloy without and with the coatings, obtained in the base electrolyte, are much lower than for AZ31 (Fig. 13 and Table 8). Evidently, corrosion processes take place under the PEO coatings obtained on AZ31. Even the corrosion current of the alloy with the thickest coating on AZ31 (about 51.3 μm) decreases by 50 times only. Taking into account that in this case most of the alloy is covered by the coating and that corrosion takes place only in regions of coating defects, this minor decrease in the corrosion current means that intensive corrosion processes occur under the coating. In contrast, the corrosion current of AZ91 with the thickest coating (about 55.4 μm) decreases by almost 600 times (Table 8). Such a coating on AZ91 demonstrates a significant improvement of the corrosion properties, which exceed the GOST 9.308–85 requirements. However, the corrosion potential of the bare AZ91 alloy is almost the same as for the one coated in the base electrolyte, thus, electrolyte still reaches the substrate and localized corrosion may take place.

However, the corrosion potential of AZ91 alloy increases by 140 mV and the corrosion current decreases by almost 1000 times after the two-step PEO treatment. Therefore, it seems that the two-step PEO treatment of AZ91 alloy results in a much denser coating which limits corrosion processes to a larger extent. However, comparing the single and two-step processes, the release of hydrogen bubbles after the same immersion time in 3 wt% NaCl aqueous solution (Table 8) in-

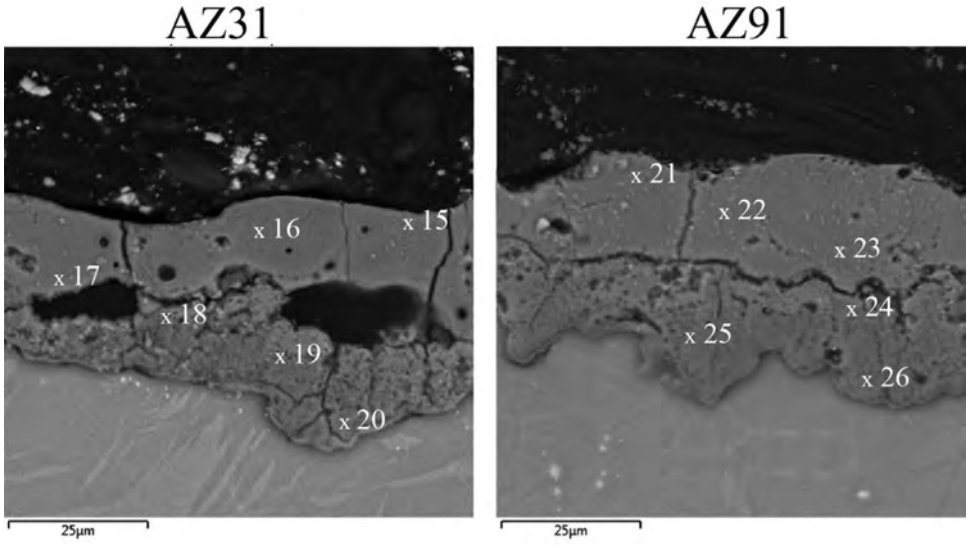


Fig. 12. Micrographs of cross-section morphology of coating obtained by the two-step PEO treatment of AZ31 (a) and AZ91 (b) alloys.

Table 5
Elemental composition of the "two-step" coatings at the locations indicated in Fig. 12.

| Element | Elemental composition, wt% | | | | | | | | | | | |
|---|---|---|---|---|---|---|---|---|---|---|---|---|
| | Point 15 | Point 16 | Point 17 | Point 18 | Point 19 | Point 20 | Point 21 | Point 22 | Point 23 | Point 24 | Point 25 | Point 26 |
| Mg | 33.6 | 36.7 | 38.4 | 48.8 | 53.9 | 56.4 | 43.1 | 42.7 | 40.9 | 43.3 | 49.9 | 45.6 |
| O | 44.6 | 41.8 | 48.6 | 39.7 | 41.4 | 40.3 | 39.1 | 40.3 | 42.5 | 44.1 | 43.5 | 40.1 |
| Al | 10.6 | 13.6 | 9.5 | 4.6 | 3.2 | 2.4 | 15.9 | 15.1 | 13.2 | 8.7 | 6.5 | 10.5 |
| P | 3.9 | 4.8 | 1.5 | 4.9 | 1.5 | 0.9 | 0.8 | 1.9 | 2.7 | 3.6 | 0.0 | 3.8 |
| Si | 7.3 | 3.1 | 2 | 2 | 0.0 | 0.0 | 1.1 | 0.0 | 0.7 | 0.3 | 0.1 | 0.0 |

Table 6
Time before release of the first hydrogen bubble and appearance of the first visible pit during immersion of AZ91 and AZ31 alloys (without and with coatings of different thicknesses produced in the base electrolyte) in 3 wt% NaCl aqueous solution.

| Alloy | Thickness, μm | Time before release of first hydrogen bubble, min | | Time before appearance of the first visible pit, min | |
|---|---|---|---|---|---|
| | | On the edges and corners | On the faces | On the edges and corners | On the faces |
| AZ31 | 0.0 | Up to 0.02 | Up to 0.02 | 5.0 ± 2.0 | 15.0 ± 4.0 |
| | 17.4 ± 2.3 | 16.0 ± 1.5 | 664.0 ± 30.0 | 27.0 ± 4.0 | 1050.0 ± 110.0 |
| | 45.2 ± 3.5 | 20.0 ± 6.0 | 315.0 ± 45.0 | 45.0 ± 25.0 | 620.0 ± 150.0 |
| | 53.0 ± 4.9 | 51.0 ± 4.0 | 936.0 ± 80.0 | 110.0 ± 20.0 | 1260.0 ± 120.0 |
| AZ91 | 0.0 | Up to 0.02 | Up to 0.02 | 14.0 ± 3.0 | 35.0 ± 5.0 |
| | 19.5 ± 3.1 | 126.0 ± 28.0 | 620.0 ± 48.0 | 240.0 ± 70.0 | 820.0 ± 130.0 |
| | 53.5 ± 3.5 | 1430.0 ± 59.0 | 1500.0 ± 30.0 | 1560.0 ± 58.0 | No pits were found during 1800 min of exposure |
| | 56.5 ± 4.6 | 1430.0 ± 50 | 1560.0 ± 90.0 | 1680.0 ± 150.0 | No pits were found during 1800 min of exposure |

Table 7
Time before release of the first hydrogen bubble and appearance of the first visible pit during immersion of coated AZ91 and AZ31 alloys (by two-step PEO treatment) in 3 wt% NaCl aqueous solution.

| Alloy | Thickness, μm | Time before release of first hydrogen bubble, min | | Time before appearance of first visible pit, min | |
|---|---|---|---|---|---|
| | | On the edges and corners | On the faces | On the edges and corners | On the faces |
| AZ31 | 43.7 ± 3.7 | 54.0 ± 7.0 | 690.0 ± 30.0 | 140.0 ± 20.0 | 1320.0 ± 180.0 |
| AZ91 | 45.4 ± 4.7 | 1420.0 ± 55.0 | 1560.0 ± 90.0 | 1740.0 ± 120.0 | No pits were found during 1800 min of exposure |

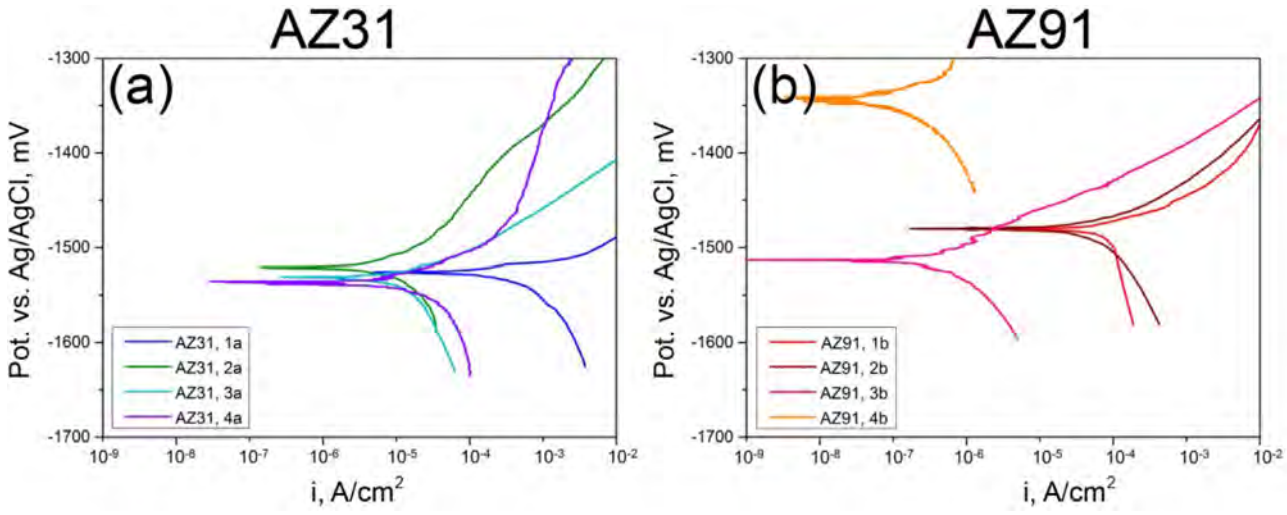


Fig. 13. Potentiodynamic polarization curves recorded for AZ31 (a) and AZ91(b) alloys during the immersion in 3 wt% NaCl aqueous solution without (1a, 1b) and with coatings obtained in the base electrolyte with an average coating thicknesses of 21 (2a), 51 (3a), 21 (2b), 55 (3b) μm or by the two-step PEO process with an average coating thicknesses of 44 (4a), 46 (4b) μm.

Table 8
Corrosion currents and potentials of AZ31 and AZ91 alloys with and without PEO coatings during immersion in 3 wt% NaCl aqueous solution.

| Alloy | Coating thickness, μm | $i$, A/cm$^2$ | $-V$, mV |
|---|---|---|---|
| AZ31 | 0.0 | $1.0 \cdot 10^{-4}$ | 1525 |
| AZ31 | 21.3 ± 3.4 | $4.0\ 10^{-6}$ | 1520 |
| AZ31 | 51.3 ± 4.4 | $2.0 \cdot 10^{-6}$ | 1530 |
| AZ31 after two-step PEO treatment | 44.1 ± 3.8 | $3.0 \cdot 10^{-6}$ | 1535 |
| AZ91 | 0.0 | $3.0 \cdot 10^{-5}$ | 1480 |
| AZ91 | 21.2 ± 3.6 | $7.5 \cdot 10^{-6}$ | 1480 |
| AZ91 | 55.4 ± 4.7 | $5.0 \cdot 10^{-8}$ | 1495 |
| AZ91 after two-step PEO treatment | 45.9 ± 4.7 | $3.0 \cdot 10^{-8}$ | 1340 |

dicates that corrosion processes still occur but only in very few places on the metal substrate.

Overall, the corrosion resistance of the coatings obtained on AZ31 alloy with different thicknesses is still not sufficient. However, due to their remaining porosity, they can be loaded with inhibitors [69] or/and sealed with paints and varnishes to obtain active corrosion protection system [70–74]. Up to now, only the corrosion properties of the coatings obtained on AZ91 fulfill the GOST 9.308–85 requirements. However, the released hydrogen bubbles (Table 7) suggest that the remaining pores and defects should also be loaded with inhibitors or/and sealed with paints and varnishes to eliminate localized corrosion of the metal substrate.

## 4. Conclusions

(1) A mechanism of initial formation of horizontal pores during PEO processes in alkali-phosphate-aluminate electrolyte was proposed. On the bottom of those horizontal pores, formation of an anodic film and its dissolution take place. Thus, the further continuation of PEO processing leads to ignition of microdischarges under the outer layer of the coating grown on AZ91 and AZ31 alloys. Three-layer coatings are formed: an anodic film, an inner and an outer layer.

(2) The growth of outer and inner layers of PEO coatings occurs via different mechanisms. Due to high-energy microdischarges in vertical pores of the coating and spherical voids inside the coating, the formation of a melted porous outer layer occurs. The growth of the inner layer of the coatings is more complicated and consists of:
   (i) anodizing with formation and dissolution of a porous film on the metal surface;
   (ii) formation of horizontal pores as a result of a dissolution process, which partially separate the anodic film from the metal substrate;
   (iii) sealing of the pores in the anodic film by gas-vapor phase, followed by microdischarges, resulting in the formation of the inner layer of PEO coating;
   (iv) dissolution of the oxides circumjacent to the horizontal pores with simultaneous appearance of microdischarges in the pores of the inner layer, promoting the formation of MgO and $MgAl_2O_4$ in these pores. As a result, the horizontal pores located between the inner and outer layers of the coating are partly sealed.

(3) The growth of coatings on both AZ31 and AZ91 alloys occurs due to appearance of three types of microdischarges taking place in the vertical, spherical and inner layer horizontal pores which reach the metal substrate. However, each type of microdischarge releases different amount of energy. Higher energy is emitted at narrow volumes of vertical curved pores, leading to the formation of spheric pores in the PEO coating on AZ31 alloy. For this reason, the coatings formed on AZ31 alloy are more porous in comparison with AZ91 alloy.

(4) Only thick (53.5–56.5 μm) coatings obtained on the AZ91 alloy and coatings obtained by a two-step PEO treatment of this alloy demonstrate high corrosion resistance.

## Declaration of Competing Interests

No conflict of interests in regards to the presented work can be declared.

## Acknowledgments

The authors would like to thank ACTICOAT project in frame of Era.NET-Rus+Call, 2017 (Project N477) and RFBR (Project No. 18-53-76008) in the frame of project ACTICOAT (Era.Net RUS Plus Call 2017, Project 477) for the partial financial support of this work. MS, MZ and CB additionally appreciate European project FUNCOAT ("Development and design of novel multiFUNctional PEO COATings" in frame of H2020-MSCA-RISE-2018 call, Grant Agreement No 823942) for the financial assistance.

## References

[1] S.V. Gnedenkov, S.L. Sinebriukhov, V.I. Sergienko, Multifunctional Composite Coatings on Metals and Alloys Formed by Plasma Electrolytic Oxidation *[Kompozicionnye Mnogofunkcional'nye Pokrytiya na Metallah i Splavah, Formiruemye Plazmenno – Elektroliticheskim Oksidirovaniem]*, 460, Dal'nauka, Vladivostok, 2013 ISBN: 978-5-8044-1398-0 *(in Russian)*.

[2] Barati Darband Gh., Aliofkhazraei M., P. Hamghalam, N. Valizade, J. Magnes. Alloys 5 (1) (2017) 74–132, doi:10.1016/j.jma.2017.02.004.

[3] J. Zhang, S. Yan, H. Qu, Int. J. Hydrogen Energy. 42 (26) (2017) 16603–16610, doi:10.1016/j.ijhydene.2017.05.174.

[4] L.A. Snezhko, V.S. Rudnev, M. Tehnika (Ed.), Anodic Spark Oxidation of Magnesium *[Anodno-Iskrovoe Oksidirovanie Magniya]*, 160, 2014 ISBN 5-93969-047-5 *(in Russian)*.

[5] S. You, Y. Huang, K.U. Kainer, N. Hort, J. Magnes. Alloys 5 (3) (2017) 239–252, doi:10.1016/j.jma.2017.09.001.

[6] B. Song, N. Guo, T. Liu, Q. Yang, Mater. Des. 62 (2014) 352–360, doi:10.1016/j.matdes.2014.05.034.

[7] L. Ren, et al., Int. J. Lightw. Mater. Manuf. 1 (2) (2018) 81–88, doi:10.1016/j.ijlmm.2018.05.002.

[8] O. Khaselev, D. Weiss, J. Yahalom, J. Electrochem. Soc. 146 (5) (1999) 1757–1761, doi:10.1149/1.1391838.

[9] X. Lu, et al., Surf. Coat. Technol. 307 (2016) 1165–1182, doi:10.1016/j.surfcoat.2016.08.055.

[10] W. Chen, Z. Wang, L. Sun, S. Lu, J. Magnes. Alloys 3 (3) (2015) 253–257, doi:10.1016/j.jma.2015.07.003.

[11] Z. Shahri, S.R. Allahkaram, R. Soltani, H. Jafari, J. Magnes. Alloys (2018), doi:10.1016/j.jma.2018.10.001.

[12] Z. Ur Rehman, D. Choi, J. Magnes. Alloys 7 (4) (2019) 555–655, doi:10.1016/j.jma.2019.10.001.

[13] V. Dehnavi, W.J. Binns, J.J. Noël, D.W. Shoesmith, B.L. Luan, J. Magnes. Alloys 6 (3) (2018) 229–237, doi:10.1016/j.jma.2018.05.008.

[14] C.-Y. Li, X.-L. Fan, L. Cui, R.-C. Zeng, Corros. Sci. 168 (2020), doi:10.1016/j.corsci.2020.108570.

[15] Z.-Y. Ding, et al., J. Alloys Compd. 764 (2018) 250–260, doi:10.1016/j.jallcom.2018.06.073.

[16] S.L. Sinebrjuhov, et al., Prot. Metals Phys. Chem. Surf. 48 (6) (2012) 579–588, doi:10.1134/S2070205112060147.

[17] J. Martin, et al., Mater. Des. 178 (2019) 107859, doi:10.1016/j.matdes.2019.107859.

[18] A.G. Rakoch, A.V. Dub, A.A. Gladkova, M. Staraja Basmannaja (Ed.), Anodizing of Light Alloys under Various Electrical Modes. Plasma Electrolytic Nanotechnology. *[Anodirovanie legkih splavov pri Razlichnyh Elektricheskih Rezhimah. Plazmenno-Elektroliticheskaya Nanotekhnologiya]*, 495, 2012 ISBN 978-5-904043-82-7 *(in Russian)*.

[19] A.G. Rakoch, A.A. Gladkova, A.V. Dub, M. MISiS (Ed.), Plasma electrolytic Treatment of Aluminum and Titanium Alloys *[Plazmenno–elektroliticheskaya obrabotka alyuminievyh i titanovyh splavov]*, 160, 2017 ISBN 978-5-906846-51-8 *(in Russian)*.

[20] I.V. Suminov, et al., in: M. Tehnosfera (Ed.), Plasma Electrolytic Surface Modification of Metals and Alloys *[Plazmenno–Elektroliticheskoe Modificirovanie Poverhnosti Metallov i Splavov]*, 512, 2011, p. 2. ISBN 978-5-94836-266-3 *(in Russian)*.

[21] W. Tu, et al., J. Alloy Compd. 725 (2017) 199–216, doi:10.1016/j.jallcom.2017.07.117.

[22] P.H. Sobrinho, Y. Savguira, Q. Ni, S.J. Thorpe, Surf. Coat. Technol. 315 (2017) 530–545, doi:10.1016/j.surfcoat.2017.02.029.

[23] F. Zhu, J. Wang, S. Li, J. Zhang, Appl. Surf. Sci. 258 (2012) 8985–8990, doi:10.1016/j.apsusc.2012.05.135.

[24] S. Yagi, A. Sengoku, K. Kubota, E. Matsubara, Corros. Sci. 57 (2012) 74–80, doi:10.1016/j.corsci.2011.12.032.

[25] M. Boinet, S. Verdier, S. Maximovitch, F. Dalard, Electrochem. Prop. Coat. Surf. Coat. Technol. 199 (2–3) (2005) 141–149, doi:10.1016/j.surfcoat.2004.10.145.

[26] A. Günther-Schulze, H Betz, Z. Phys. 78 (1932) 196–210.

[27] A. Günther-Schulze, H Betz, Electrolytic Capacitors *[Elektroliticheskie Kondensatory]*, 200, MOborongiz, 1938 *(in Russian)*.

[28] A.G. Rakoch, V.V. Hohlov, V.A. Bautin, N.A. Lebedeva, J.V. Magurova, Protect. Metals (Zashch. Metal.) 42 (2) (2006) 173–184 ISSN: 0033-1732eISSN: 1608-327X *(in Russian)*, doi:10.1134/s003317320602010x.

[29] A.G. Rakoch, I.V. Bardin, V.L. Kovalev, T.G. Avanesjan, Izvest. VUZov 2 (2011) 58–62 ISSN: 1997-308XeISSN: 2412-8767 *(in Russian)*.

[30] Y.Q. Wang, X.J. Wang, T. Zhang, K. Wu, F.H. Wang, J. Mater. Sci. Technol. 29 (2013) 1129–1133, doi:10.3103/S1068375514030090.

[31] Y. Chen, Y. Yang, W. Zhang, T. Zhang, F. Wang, J. Alloys Compd. 718 (2017) 92–103, doi:10.1016/j.jallcom.2017.05.010.

[32] R.F. Zhang, S.F. Zhang, Corros. Sci. 51 (2009) 2820–2825, doi:10.1016/j.corsci.2009.08.009.

[33] S.F. Zhang, R.F. Zhang, W.K. Li, M.S. Li, G.L. Yang, Surf. Coat. Technol. 207 (2012) 170–176, doi:10.1016/j.surfcoat.2012.06.056.

[34] O. Khaselev, D. Weiss, J. Yahalom, Corros. Sci. 43 (2001) 1295–1307, doi:10.1016/S0010-938X(00)00116-5.

[35] K.M. Lee, Y.G. Ko, D.H. Shin, Thin Solid Films. 531 (2013) 261–265, doi:10.1016/j.tsf.2013.01.008.

[36] K.C. Tekin, U. Malayoglu, S. Shrestha, Surf. Coat. Technol. 236 (2013) 540–549, doi:10.1016/j.surfcoat.2013.10.051.

[37] C. Liu, et al., J. Alloys Compd. 784 (2019) 414–421, doi:10.1016/j.jallcom.2019.01.095.

[38] P. Wang, J. Li, Y. Guo, Z. Yang, J. Rare Earth 28 (2010) 798–802.

[39] M. Mohedano, R. Arrabal, B. Mingo, A. Pardo, E. Matykina, Surf. Coat. Technol. 334 (2018) 328–335, doi:10.1016/S1002-0721(09)60204-0.

[40] D.V. Mashtalyar, S.V. Gnedenkov, S.L. Sinebryukhov, I.M. Imshinetskiy, A.V. Puz, J. Mater. Sci. Technol. 33 (2017) 461–468, doi:10.1016/j.jmst.2017.01.021.

[41] R. Arrabal, et al., Appl. Surf. Sci. 254 (2008) 6937–6942, doi:10.1016/j.apsusc.2008.04.100.

[42] K.M. Lee, K.R. Shin, S. Namgung, B. Yoo, D.H. Shin, Surf. Coat. Technol. 205 (2011) 3779–3784, doi:10.1016/j.surfcoat.2011.01.033.

[43] K.M. Lee, et al., Electrochim. Acta 67 (2012) 6–11, doi:10.1016/j.electacta.2012.01.053.

[44] M. Tang, H. Liu, W. Li, L. Zhu, Mater. Lett. 65 (2011) 413–415, doi:10.1016/j.matlet.2010.09.041.

[45] S.V. Gnedenkov, et al., Vacuum. 120 (2015) 107–114, doi:10.1016/j.vacuum.2015.02.004.

[46] T.S. Lim, H.S. Ryu, S.H. Hong, Corros. Sci. 62 (2012) 104–111, doi:10.1016/j.corsci.2012.04.043.

[47] Y. Xiong, C. Lu, C. Wang, R. Song, Appl. Surf. Sci. 322 (2014) 230–235, doi:10.1016/j.apsusc.2014.10.103.

[48] M. Mohedano, C. Blawert, M.L Zheludkevich, Mater. Des. 86 (2015) 735–744, doi:10.1016/j.matdes.2015.07.132.
[49] F. Tjiang, et al., Ceram. Int. 43 (1) (2017) S567–S572, doi:10.1016/j.ceramint.2017.05.179.
[50] R.O. Hussein, D.O. Northwood, X. Nie, Surf. Coat. Tech. 237 (2013) 357–368, doi:10.1016/j.surfcoat.2013.09.021.
[51] F. Liu, et al., Mater. Chem. Phys. 162 (2015) 452–460, doi:10.1016/j.matchemphys.2015.06.014.
[52] M. Sun, A. Matthews, A. Yerokhin, Surf. Coat. Technol. 344 (2018) 330–341, doi:10.1016/j.surfcoat.2018.02.078.
[53] A. Jangde, S. Kumar, C. Blawert, Corros. Sci. 157 (2019) 220–246, doi:10.1016/j.corsci.2019.05.024.
[54] P.B. Srinivasan, et al., Appl. Surf. Sci. 256 (12) (2010) 4017–4022, doi:10.1016/j.apsusc.2010.01.069.
[55] J. Liang, et al., Electrochim. Acta. 54 (14) (2009) 3842–3850, doi:10.1016/j.electacta.2009.02.004.
[56] P.B. Srinivasan, et al., Appl. Surf. Sci. 255 (7) (2009) 4212–4218, doi:10.1016/j.apsusc.2008.11.008.
[57] J. Liang, P.B. Srinivasan, C. Blawert, W. Dietzel, Corros. Sci. 51 (10) (2009) 2483–2492, doi:10.1016/j.corsci.2009.06.034.
[58] A.G. Rakoch, A.A. Gladkova, Z. Linn, D.M. Strekalina, Surf. Coat. Technol. 269 (2015) 138–144, doi:10.1016/j.surfcoat.2015.02.026.
[59] M. Stern, A.L. Geary, J. Electrochem. Soc. 104 (1957) 56, doi:10.1149/1.2428496.
[60] C. Blawert, S.A. Karpushenkov, M. Serdechnova, L.S. Karpushenkava, M.L. Zheludkevich, Appl. Surf. Sci. (2019), doi:10.1016/j.apsusc.2019.144552.
[61] N.D. Tomashov, F.P. Zalivalov, M.N. Tjukina, Thick-Layer Anodizing of Aluminum and its Alloys [*Tolstoslojnoe Anodirovanie Alyuminiya i Ego Splavov*], 220, Mashinostroenie, 1968 (*in Russian*).
[62] L. Cancan, Z. Hui, G. Xin, J. Bailing, L. Jun, J. Alloy Compd. 770 (2019) 500–506, doi:10.1016/j.jallcom.2018.08.141.
[63] D.A. Vermilyea, C.F. Kirk, Studies of inhibition of magnesium corrosion, J. Electrochem. Soc. 116 (1969) 1487–1492.
[64] A.P. Babichev, N.A. Babushkina, A.M. Bratkovskiy, et al. Physical Quantities: Reference [Fizicheskiye Velichiny: Spravochnik]. 1332, Energoatomizdat, 1991. (*in Russian*), ISBN: 5 -283-04013-5.
[65] I.A. Kozlov, S.S. Vinogradov, Z.P. Uridiya, V.A. Duyunova V.A., V.A. Manchenko, in: Trudy VIAM: Elektron. Nauch.-Tekhnich. Zhurn. (Proceedings of VIAM: Electron. Scientific and Technical Journal), 9, 2018, pp. 32–42, doi:10.18577/2307-6046-2018-0-9-32-42.
[66] I.A. Kozlov, S.S. Vinogradov, S.A. Naprienko, Korroz.: Mater. Zashch. (Corros.: Mater. Protect.) 8 (2017) 37–48 *(in Russian)*.
[67] J.A. Curran, T.W. Clyne, Acta Mater 54 (7) (2006) 1985–1993, doi:10.1016/j.actamat.2005.12.029.
[68] GOST 9.308-85, Metals Non-metal Inorg. Coat. (1987) Methods for accelerated corrosion test", opened at 01.01.1987.
[69] A.A. Chirkunov, A.G. Rakoch, E.V. Monakhova, A.A. Gladkova, Z.V. Khabibullina, V.A. Ogorodnikova, M. Serdechnova, C. Blawert, Yu.I. Kuznetsov, M.L. Zheludkevich, Int. J. Corros. Scale Inhibi. 8 (4) (2019) 1170–1188, doi:10.17675/2305-6894-2019-8-4-22.
[70] Z.H. Wan, J.M. Zhang, Y. Li, L.J. Bai-jing, G.J. Zhang, Trans. Nonferrous Metals Soc. China 29 (10) (2019) 2066–2077, doi:10.1016/S1003-6326(19)65113-7.
[71] D.K. Ivanou, M. Starykevich, A.D. Lisenkov, M.L. Zheludkevich, H.B. Xue, S.V. Lamaka, M.G.S. Ferreira, Corros. Sci. 73 (2013) 300–308, doi:10.1016/j.corsci.2013.04.019.
[72] J. Yang, C. Blawert, S.V. Lamaka, D. Snihirova, X. Lu, S. Di, M.L. Zheludkevich, Corros. Sci. 140 (2018) 99–110, doi:10.1016/j.corsci.2018.06.014.
[73] Y. Chen, X. Lu, S.V. Lamaka, P. Ju, C. Blawert, T. Zhang, F. Wang, M.L. Zheludkevich, Appl. Surf. Sci., 10.1016/j.apsusc.2019.144462.
[74] D.K. Ivanou, K.A. Yasakau, S. Kallip, A.D. Lisenkov, M. Starykevich, S.V. Lamaka, M.G.S. Ferreira, M.L. Zheludkevich, RSC Adv. 6 (2016) 12553–12560, doi:10.1039/C5RA22639B.